URSI AP-RASC, Sydney, Australia, 17 – 22 August 2025

Analysis of Ionospheric ROTI Variations over South East Asia Using SiReNT data

Pasumarthi Babu Sree Harsha and Koen Mouthaan
Department of Electrical and Computer Engineering, National University of Singapore, Singapore

Abstract

Ionospheric rate of total electron content (TEC) index (ROTI) values are generated and analyzed for detection and assessment of possible equatorial plasma bubbles in the Southeast Asia region. The potential of the Singapore satellite positioning reference network (SiReNT) GNSS receivers for this purpose is explored. The 1 Hz sampling GNSS data from November 2021 to July 2022 is processed to determine various ionospheric parameters and estimation of 5-minute ROTI values is investigated. Keogram analysis of ROTI from $1°S$ to $3°N$ is presented for 22 and 23 May 2022. Additionally, the normalized ROTI values are estimated over different geographic latitudes. The maximum normalized ROTI values are observed over the $0°N$ latitudes. Equatorial plasma bubble-like striations for the respective days are found and analyzed.

1 Introduction

Trans-ionospheric propagation can be severely disrupted by small-scale ionospheric irregularities along satellite-to-ground signal links. These irregularities can induce severe position errors when using global navigation satellite systems (GNSS) and create challenges for critical applications. One of the parameters that is widely used to better understand ionospheric irregularities is the rate of TEC index (ROTI) [1]. Several researchers have used ROTI as a reliable index to investigate and assess temporal variations of ionospheric irregularities [2].

Throughout the past three decades, GNSS measurements have become vital in understanding equatorial plasma bubbles (EPB) [3], [4]. A network of GNSS receivers distributed over a geographical region can help in measuring the spatial variability of ROTI. In particular, there are critical challenges in the predictive capabilities of EPBs over the Southeast Asia (SEA) region. These are presumed to be field-aligned irregularities with two-dimensional structures. SEA is more prone to such multi-scale plasma instabilities ranging from a few meters to hundreds of kilometers in size [5], [6]. Various observation techniques have been proposed to understand the seeding, generation, and propagation of the ionospheric irregularities including airglow imagers, incoherent scatter radars, ionosondes, GPS and other in situ measurements [4], [7].

Unseasonal generation of EPBs over SEA was observed with lower ROTI values linked to non-linear effects and shielding effects in [8].

Nishioka et al. conducted global positioning system (GPS) TEC measurements over SEA to investigate the occurrence of latitudinal and longitudinal variations of EPBs [9]. Buhari et al. used 127 stations in SEA to create two-dimensional ROTI maps [10]. A comparative study using GPS ROTI with an airglow imager and equatorial atmosphere radar (EAR) have also been carried out [10].

Here, results of keogram analysis are presented using data from the Singapore satellite positioning reference network (SiReNT) GNSS network in Singapore to study the ionospheric impacts over part of SEA and to understand EPBs.

2 SiReNT Data

SiReNT provides post-processed receiver independent exchange (RINEX) data for eight receiver stations distributed over Singapore. Fig.1 provides the location of the eight SiReNT GNSS receivers (blue triagles). The sampling frequency of the GNSS data is 1 Hz and the associated RINEX files are organized by station, year, month, and day. GNSS observables, such as pseudorange, carrier phase, Doppler shift, and carrier-to-noise (C/No) ratio, are extracted for each station for all satellite constellations. The processed RINEX data is stored as Level-0 database files for further analysis using an in-house developed Python package designed for GNSS data extraction.

Precise orbit information is appended to the Level-0 database by retrieving SP3 (Standard Product Version 3.0) files for each respective day from the Crustal Dynamics Data Information System (CDDIS) [11]. The satellite ECEF (x, y, z) coordinates from the SP3 files are provided at 5-minute intervals and are interpolated to 30-second resolution to align precisely with GNSS observables in the Level-0 database.

ECEF coordinates are then transformed into elevation, azimuth, and range values. Using the geographic latitude and longitude of each station, the respective ionospheric pierce points (IPPs) are estimated based on a thin-shell ionospheric height approximation of 350 km [12]. The phase-leveled code method [13] is implemented to compute slant total electron content (STEC) values for each satellite

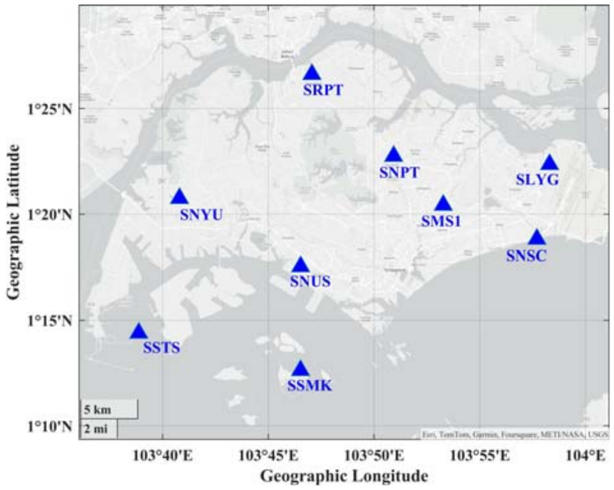

Figure 1. Geographic locations of SiReNT GNSS receivers in Singapore used for ROTI estimation.

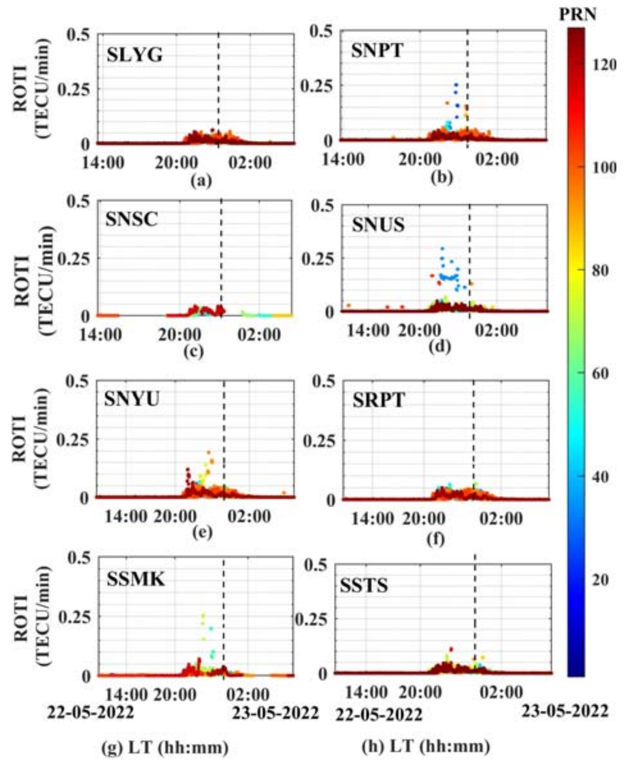

Figure 2. (a)-(h) Daily rate of TEC index (ROTI) variations for eight SiReNT stations for 22 and 23 May 2022. The colorbar represents pseudo random number (PRN) for the multi-constellation satellite systems (GPS, GLONASS, GALILEO, BEIDOU, and QZSS). The dashed line on each subplot indicates the local mid-night timestamp (LT = UTC+8 hours).

arc, utilizing dual-frequency carrier phase and pseudorange measurements.

Cycle-slip detection is applied to resolve integer ambiguity in carrier phase observations. Furthermore, a thresholding method is used to detect cycle slips, and satellite arcs shorter than 20 minutes are rejected to minimize large leveling errors. ROTI values are then computed from STEC measurements at 5-minute intervals, and the uncalibrated STEC values are appended to the Level-0 database. The Level-1 database files are generated by systematically organizing daily, station-wise, and time-wise datasets, which include GNSS observables, orbit parameters, IPP coordinates, STEC and ROTI measurements. Finally, Level-2 products of temporal STEC and ROTI for each day are stored for research and visualization.

The RINEX files are accessed for all the receivers from November 2021 to July 2022. ROTI values are estimated for 5 minute intervals for each station-satellite pair.

3 Methodology

The ambiguity resolved carrier phase measurements is obtained for each satellite-station pair using [13]:

$$\begin{aligned}\tilde{P}^{s}_{r,4} &= \phi^{s,k}_{r,4} - \frac{1}{n}\sum_{k=1}^{n}\left(\phi^{s,k}_{r,4} + P^{s,k}_{r,4}\right) \\ &= -\left(\gamma_{L1} - \gamma_{L2}\right)\cdot I + c\cdot\left(\mathrm{DCB}^{k}_{r,L1,L2} + \mathrm{DCB}^{s,k}_{L1,L2}\right) \quad (1)\end{aligned}$$

where c is the velocity of light (299 792 458 m/s), $\tilde{P}^{s}_{r,4}$ is the uncalibrated slant TEC measurement (TEC(n)), $P^{s,k}_{r,4}$ and $\phi^{s,k}_{r,4}$ are the geometry free combination of dual-frequency pseudorange and carrier phase measurements for each satellite (superscript s) and receiver (subscript r), k is the total number of measurements in the arc of the particular satellite s, n is the epoch in the particular satellite-arc, I is the differential ionospheric delay of L1 and L2 frequencies for the particular constellation, $\gamma_{L1} = \left(\frac{f_0}{f_{L1}}\right)^2$ and $\gamma_{L2} = \left(\frac{f_0}{f_{L2}}\right)^2$ denote the ratio of ionospheric delay of f_{L1} and f_{L2} with fundamental frequency f_0, $\mathrm{DCB}^{k}_{r,L1,L2}$, and, lastly, $\mathrm{DCB}^{s,k}_{L1,L2}$ are the receiver and satellite differential code biases, respectively.

The rate of total electron content (ROT) is given by,

$$\mathrm{ROT} = \frac{\mathrm{TEC}(n+\Delta n) - \mathrm{TEC}(n)}{\Delta n} \quad (2)$$

where, Δn is the next time epoch of the satellite.

ROTI is estimated using [1]:

$$\mathrm{ROTI} = \sqrt{\langle \mathrm{ROT}^2 \rangle - \langle \mathrm{ROT} \rangle^2} \quad (3)$$

ROTI values are estimated through a sliding window of 5 minutes for all the respective stations. The estimated day-wise ROTI values are utilized for further study. Normalized ROTI is computed for each satellite from the ROTI values in (3):

$$\mathrm{ROTI}_{Norm} = \frac{\mathrm{ROTI}}{\max(\mathrm{ROTI})} \quad (4)$$

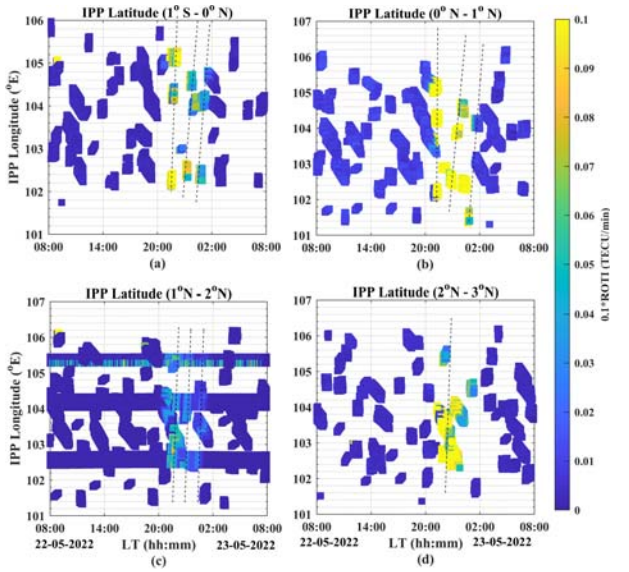

Figure 3. ROTI keogram for different IPP latitudes. (a) $1°S$ - $0°N$. (b) $0°N$ - $1°N$. (c) $1°N$ - $2°N$. (d) $2°N$ - $3°N$. Dotted lines indicate possible elongated striations due to EPBs.

4 Results and Discussion

The ROTI variation for each station is computed for 22 May and 23 May 2022 and shown in Fig. 2 by considering an elevation cut-off of 50° to avoid urban multipath effects (Eq. (3)). Most of the stations have a increment in ROTI values gradually after post-sunset to mid-night hours on 22 May 2022. The SNUS and SNPT stations have peak ROTI values of about 0.3 TECU/min, around 21:00 LT suggesting the occurrence of regular EPBs over the equatorial region. The ROTI keogram is visualized for four different latitudinal groups (Fig. 3). The local time is on the x-axis and the y-axis is the estimated IPP longitude of all the station data for the day. The colorbar represents the 0.1 times the ROTI values (Eq. (3)).

Fig. 3(a)-(d) shows IPP latitudinal groups between $1°S$ and $0°N$. Three meridionally elongated striations (shown as dotted lines), spanning from $102°E$ to $106°E$, could be associated with EPBs. Each striation has a lifespan of approximately three hours. Buhari et al. previously reported EPB lifespans ranging from 50 minutes to 7 hours over the SEA region [10]. The growth and lifespan of EPBs depend on non-linear effects associated with localized and external forces. Additionally, unseasonal EPBs have been observed during periods of low solar activity, as reported in earlier studies [8].

Normalized ROTI values of the common time stamps between the four latitudinal groups are selected. Fig. 4 depicts the temporal variation of normalized ROTI values for the respective latitudinal groups. All the latitudinal groups have high ROTI values between 21:00 LT to 24:00 LT on 22 May 2022. Using the normalized ROTI it is determined that the EPB's have higher strength over $0°N$ latitudes and

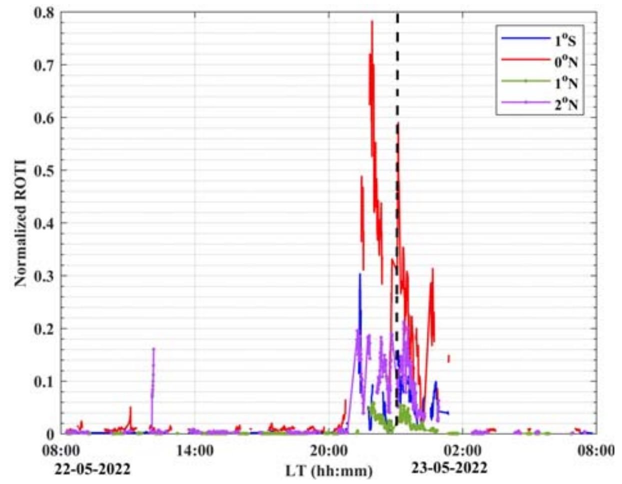

Figure 4. Estimated normalized ROTI values for 22 May and 23 May 2022 for different geographic latitudes. The dashed line indicates the local mid-night timestamp.

gradual decrease to further extension of latitudinal groups i.e. $1°S$ and $1°N$ to $2°N$, respectively. Detection of these unseasonal EPBs over SEA using the current GNSS network of receivers could be useful for improvement in the prediction capabilities of the localized irregularities prediction.

5 Conclusion

The use of SiReNT GNSS network data to investigate the capability to observe the impact of EPBs over SEA region is presented. With the SiReNT data, ROTI keograms and normalized ROTI maps over SEA can be generated, especially surrounding the geographic latitudes of $2°S$ to $2°N$ and geographic longitudes of $101°E$ to $107°E$. The SiReNT receivers are relatively closely spaced over Singapore with lower baseline distances, which is useful for better spatial understanding of EPBs. In future, climatological research for ROTI keograms is planned to understand the life-span of EPBs over the SEA region through predictive approaches.

6 Acknowledgements

This research is supported by the Office for Space Technology & Industry (OSTin) of the Economic Development Board, Singapore.

References

[1] X. Pi, A. Mannucci, U. Lindqwister, and C. Ho, "Monitoring of global ionospheric irregularities using the worldwide gps network," *Geophysical Research Letters*, vol. 24, no. 18, pp. 2283–2286, 1997.

[2] I. Cherniak, A. Krankowski, and I. Zakharenkova, "Roti maps: a new igs ionospheric product characterizing the ionospheric irregularities occurrence," *Gps Solutions*, vol. 22, pp. 1–12, 2018.

[3] T. L. Beach and P. M. Kintner, "Simultaneous global positioning system observations of equatorial scintillations and total electron content fluctuations," *Journal of Geophysical Research: Space Physics*, vol. 104, no. A10, pp. 22553–22565, 1999.

[4] Y. Otsuka, K. Shiokawa, T. Ogawa, T. Yokoyama, M. Yamamoto, and S. Fukao, "Spatial relationship of equatorial plasma bubbles and field-aligned irregularities observed with an all-sky airglow imager and the equatorial atmosphere radar," *Geophysical Research Letters*, vol. 31, no. 20, 2004.

[5] P. Abadi, I. Muafiry, T. Pratama, A. Putra, P. Suraina, W. GH, C. ST, and A. FF, "Leveraging roti map derived from indonesian gnss receiver network for advancing study of equatorial plasma bubble in southeast," *East Asia. Earth Planet. Phys*, vol. 9, no. 1, pp. 101–116, 2024.

[6] S. Basu, S. Basu, J. Aarons, J. McClure, and M. Cousins, "On the coexistence of kilometer-and meter-scale irregularities in the nighttime equatorial f region," *Journal of Geophysical Research: Space Physics*, vol. 83, no. A9, pp. 4219–4226, 1978.

[7] S. Saito, S. Fukao, M. Yamamoto, Y. Otsuka, and T. Maruyama, "Decay of 3-m-scale ionospheric irregularities associated with a plasma bubble observed with the equatorial atmosphere radar," *Journal of Geophysical Research: Space Physics*, vol. 113, no. A11, 2008.

[8] J. Currie, B. Carter, J. Retterer, T. Dao, R. Pradipta, R. Caton, K. Groves, Y. Otsuka, T. Yokoyama, K. Hozumi, *et al.*, "On the generation of an unseasonal epb over south east asia," *Journal of Geophysical Research: Space Physics*, vol. 126, no. 2, p. e2020JA028724, 2021.

[9] M. Nishioka, A. Saito, and T. Tsugawa, "Occurrence characteristics of plasma bubble derived from global ground-based gps receiver networks," *Journal of Geophysical Research: Space Physics*, vol. 113, no. A5, 2008.

[10] S. Buhari, M. Abdullah, A. Hasbi, Y. Otsuka, T. Yokoyama, M. Nishioka, and T. Tsugawa, "Continuous generation and two-dimensional structure of equatorial plasma bubbles observed by high-density gps receivers in southeast asia," *Journal of Geophysical Research: Space Physics*, vol. 119, no. 12, pp. 10–569, 2014.

[11] C. E. Noll, "The crustal dynamics data information system: A resource to support scientific analysis using space geodesy," *Advances in Space Research*, vol. 45, no. 12, pp. 1421–1440, 2010.

[12] E. D. Kaplan and C. Hegarty, *Understanding GPS/GNSS: principles and applications*. Artech house, 2017.

[13] X. Ren, J. Chen, X. Li, and X. Zhang, "Ionospheric total electron content estimation using gnss carrier phase observations based on zero-difference integer ambiguity: methodology and assessment," *IEEE Transactions on Geoscience and Remote Sensing*, vol. 59, no. 1, pp. 817–830, 2020.